Macromolecules

pubs.acs.org/Macromolecules Article

Stability of the Double Gyroid Phase in Bottlebrush Diblock Copolymer Melts

So Jung Park, Guo Kang Cheong, Frank S. Bates, and Kevin D. Dorfman*

Cite This: *Macromolecules* 2021, 54, 9063−9070 Read Online

ACCESS | Metrics & More | Article Recommendations | Supporting Information

ABSTRACT: Bottlebrush block copolymers are emerging as promising materials for designing advanced materials with a number of unique properties engendered by densely grafted architectures. We used self-consistent field theory (SCFT) to determine how the stability of the double gyroid phase in a diblock copolymer melt is affected by converting one or both of the blocks of a linear diblock copolymer to a bottlebrush architecture. For architecturally symmetric polymers, the dominant effect of the bottlebrush is increasing segregation strength, whereupon the gyroid stability regions are effectively the same as linear diblock copolymers at equivalent segregation. In contrast, architectural asymmetry produced by coil−bottlebrush block polymers significantly impacts the gyroid stability region as a result of conformational asymmetry, which promotes spontaneous curvature. Gyroid is more stable when the coil blocks are in minority domains, which relieves packing frustration at the center of the gyroid nodes than in majority domains. Our results suggest that architectural asymmetry in bottlebrush block polymers can be a powerful design tool.

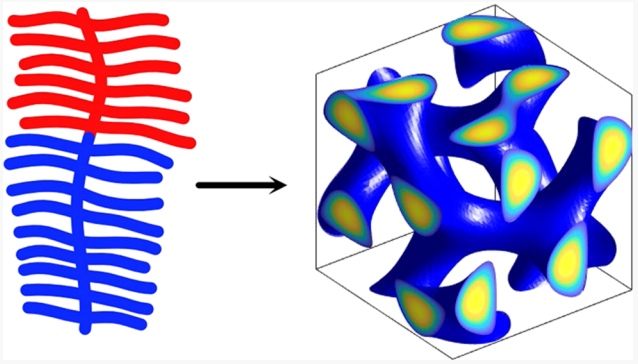

INTRODUCTION

Block polymers possess a remarkable ability to self-assemble into various ordered mesoscale structures.[1,2] With the advance of molecular synthesis techniques such as ring-opening metathesis polymerization,[3,4] bottlebrush block copolymers are emerging as a new class of branched block copolymers, which are expected to produce self-assembly behaviors unavailable in conventional diblock copolymers.[5−7] Bottlebrush block polymers consist of different types of side chains densely grafted to a high-molecular-weight linear backbone, whereupon the backbone is characterized by a highly extended conformation due to the steric congestion of the grafts.[8,9] The elongated backbone conformation and steric repulsion between grafts result in low intermolecular entanglement density in melts,[10] and this feature enables rapid self-assembly into highly ordered morphologies with large domain sizes above 100 nm,[11,12] which are hard to attain with high-molecular-weight linear diblocks. Furthermore, bottlebrush molecule shapes can be designed by the controlled placement of side chains with different lengths along the backbone. The resulting architectural variation can influence self-assembly by dictating how bottlebrush molecules pack into ordered nanostructures, as demonstrated in previous experimental research with cylindrical and spherical morphologies.[13−15] The unique self-assembly properties and tunable architectures make bottlebrush block polymers attractive candidates for creating large length-scale nanostructures useful for potential applications in photonics,[11,16−19] lithography,[20] and drug delivery.[21,22]

Most prior research has focused on producing lamella-forming bottlebrush block polymers for the fabrication of visible light photonic crystals,[11,16−19] in particular, understanding the relationship between lamellar domain spacing and backbone length.[23−26] Indeed, most bottlebrush research studies discuss the classical lamellar,[12,14,23,24,27−30] cylindrical,[13,15,28,31] and spherical phases.[14,28] It remains to be seen whether similar advances are possible for network architectures, in particular, the double gyroid phase. Network materials with scalable pore sizes are highly desirable in applications such as advanced separation membranes,[32,33] porous transport media,[34,35] and photonics.[36,37]

There has been some limited work to date on network phases in bottlebrush copolymers. Johnson and co-workers first reported the gyroid phase in A-*branch*-B Janus bottlebrush polymers, which make ultrasmall domains in their experiment, and they theoretically supported their findings using self-consistent field theory (SCFT).[38] Later, the experiments of Jiang et al. demonstrated the gyroid phase formation in compositionally gradient bottlebrush copolymers.[31] A variety

Received: August 5, 2021
Revised: September 8, 2021
Published: September 28, 2021

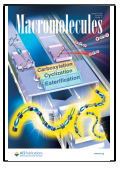

https://doi.org/10.1021/acs.macromol.1c01654
Macromolecules 2021, 54, 9063−9070

of complex network phases were explored by Lequieu et al. by performing SCFT calculations with ABC bottlebrush block polymers to find the molecular designs, which result in complete photonic band-gap structures.[39] However, these previous studies were limited to specific macromolecular architectures, like Janus and triblock bottlebrush copolymers, and a complete fundamental understanding and prediction of the stability of complex network phases for densely grafted block polymers have not been achieved yet.

In this work, we investigate the stability of double gyroid network phases in bottlebrush block copolymer melts via SCFT for the combinations of block architectures illustrated in Figure 1, focusing on how the gyroid stability regions are

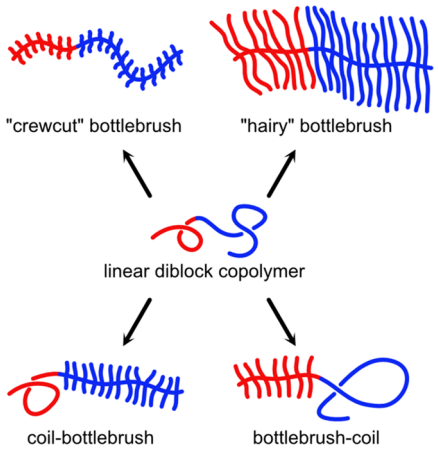

Figure 1. Schematics of block copolymer architectures consisting of linear, crewcut, or hairy blocks. All polymer models reduce to a linear AB diblock copolymer when the side-chain lengths are zero.

modified by a continuous architectural variation from linear to bottlebrush-grafted polymers. Since the most important physical principles governing phase selection of diblock copolymer melts are already well understood and confirmed by theory[40,41] and experiment,[2,42] using the diblock backbones as a starting point makes it easy to isolate the effects of the grafts on the stability of gyroid phases.

We should note that within the mean-field approximation of SCFT, the local density fluctuations on mesoscopic length scales are restricted through the incompressibility condition of the Flory–Huggins theory, and steric interactions of densely grafted side chains are completely neglected in the calculation. This implies that mean-field treatment has limitations for describing the strongly stretched backbone conformation and radially stretched side chains by the strong correlation between them. Some SCFT simulations have used wormlike chain models[24,25,43] with an adjustable persistence length to mimic the backbone stiffness induced by strong steric interaction that is not captured in the mean-field limit. For example, Dalsin et al.[24] fit their simulation data to lamellar periods measured by the experiment, demonstrating that the persistence length of the densely grafted backbone is similar to the radius of the bottlebrushes. Moreover, their work suggests that the crowding-induced backbone conformations are not highly extended, as generally supposed, but rather a considerable bending of the backbone exists away from the interface. For sufficiently long chains, the bottlebrush chain still must adopt a random walk configuration but with a persistence length that is controlled, in part, by crowding.[9] In a wormlike chain-based SCFT study of the effects of diblock copolymer rigidity on the phase diagram,[44] it was observed that when the flexibility parameter $L/2\lambda$ is 10, where L and λ are the total contour length and persistence length of the semiflexible chain, respectively, the phase diagram roughly recovers the conventional phase diagram based on the Gaussian chain model. In our calculation, we use the Gaussian chain model with assumptions that bottlebrush block polymers are very long relative to the side chains and that the impact of the steric-induced backbone rigidity is minor on the relative stability of ordered phases.[44] To simplify the problem, we focus primarily on the location of the stability window of the double gyroid phase by adopting classical lamellar, hexagonal cylinders, bcc spheres, and disorder as the candidate phases over volume fractions of the minority block that span these phases.

MODELING AND SIMULATION METHOD

Our calculations for architecturally symmetric bottlebrush models range from short (crewcut) to long (hairy) side chains, with n_{SC} = 200 of A and B side chains uniformly grafted onto the chemically identical segments of an AB diblock backbone of fixed length N_{BB}; additional calculations for n_{SC} = 100 appear in the Supporting Information (SI). The side-chain lengths are equal, $N_{SC} = N_A = N_B$, and both A and B have equal statistical segment lengths $b_A = b_B$. Architecturally asymmetric, coil–bottlebrush polymers are derived from the crewcut bottlebrush polymers by taking all A (B)-type side chains and putting them at the end of the A (B) backbone block, so that we can directly compare an architecturally symmetric crewcut bottlebrush polymer and an extremely asymmetric coil–bottlebrush polymer at the same A block composition, f_A. For the particular values of χ used in the bottlebrush calculations, all of the polymer models reduce to the linear diblock copolymer for χN = 12, where $N = N_{BB}$ as $N_{SC} \to 0$. We employed the flexible Gaussian chain model SCFT, and owing to the invariance of the model to the absolute values of N and b, we are free to choose N_{BB} = 1 and the statistical segment length b = 1 in the SCFT calculations.[45] SCFT formalism and simulation details are provided in the SI Section A. Briefly, the SCFT code used here was built on an open-source C++ implementation of PSCF software[45] developed by Morse,[46] which provides functionality for acyclic branched polymers. We have modified that code to implement the fast bottlebrush method of Levi et al.[26] using the CPU version of the C++ PSCF code. SCFT calculations were performed for lamellar, double gyroid, hexagonal cylinders and, where applicable, body-centered cubic particle phases.

RESULTS AND DISCUSSION

Architecturally Symmetric Bottlebrush Polymers. We first obtained the phase diagram of crewcut bottlebrush polymers in Figure 2 with respect to f_A and the length ratio of graft to backbone, $\alpha = N_{SC}/N_{BB}$. In the limit $\alpha \to 0$, the crewcut bottlebrush block architectures reduce to linear diblock copolymers, so the data at α = 0 correspond to diblock copolymer results at χN = 12. As α increases, the locations of phase regions shift to lower values of f_A, similar to the behavior of diblock copolymer melts when increasing χN. A similar trend in phase boundaries was reported in the study of triblock bottlebrush polymers by Lequieu et al.,[39] and they attributed the shifts to increased segregation strength due to increasing side-chain length. Taking the effect of grafts into

https://doi.org/10.1021/acs.macromol.1c01654
Macromolecules 2021, 54, 9063–9070

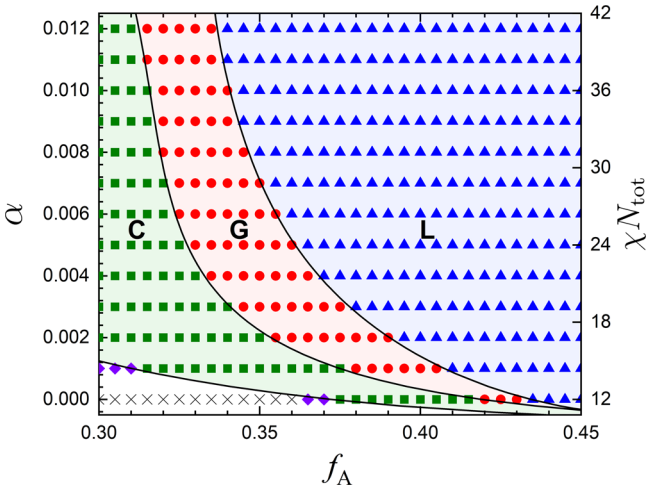

Figure 2. Phase diagram for the crewcut bottlebrush block copolymer at χ = 12 as a function of the relative length of the grafts to the backbone, α, and A block composition, f_A. The black lines are the phase boundaries of linear diblock copolymers at an equivalent $\chi N = \chi N_{tot}$, where N_{tot} is the total number of segments per bottlebrush block molecule. The stability regions of lamellar (L), hexagonal cylindrical (C), and double gyroid (G) phases are labeled, and the purple diamond and black cross-mark symbols denote the bcc spherical phase and homogeneous disordered phase, respectively.

consideration, we assumed that the effective segregation strength of the crewcut bottlebrush polymer is χN_{tot}, where $N_{tot} = N_{BB} + n_{SC}N_{SC}$ is the total number of segments. Comparing the bottlebrush results with diblock copolymer phase boundaries (solid lines in Figure 2) obtained at an equivalent $\chi N = \chi N_{tot}$ reveals that the locations of phase regions are almost identical over the parameter space examined. The results are almost independent of the graft density as shown in Figure S2 for n_{SC} = 100 and 80 side chains but the generality of χN_{tot} as a measure of segregation strength breaks down at relatively high α, exhibiting deviations from the linear diblock copolymer phase boundaries.

Going beyond the comparison of the phase diagrams, a detailed inspection of the free energy shows little difference between linear diblock copolymers and crewcut bottlebrush polymers at equivalent values of χN_{tot} (Figure S4). Moreover, we find that even the segmental probability densities are similar for bottlebrush diblock copolymers and linear diblock copolymers at equivalent values of χN_{tot}. This behavior is simplest to see for the lamellar morphology, as shown in Figure 3. Here, $P^{(j)}_{SC,A}(z, s)$ is defined as the probability distribution function of each segment in the jth grafted A-type side chain, where s = 0 at the free ends, $s = N_{SC}$ at the grafting points, and j starts from the side chain nearest to the backbone end. For $P_{BB,A}(z, s)$ of the linear diblock copolymers, the contour variable s = 0 at the A end and $s = N = N_{BB}$ at the B end. The probability distribution for each segment is normalized such that the spatial integral over one unit cell is the lamellar period

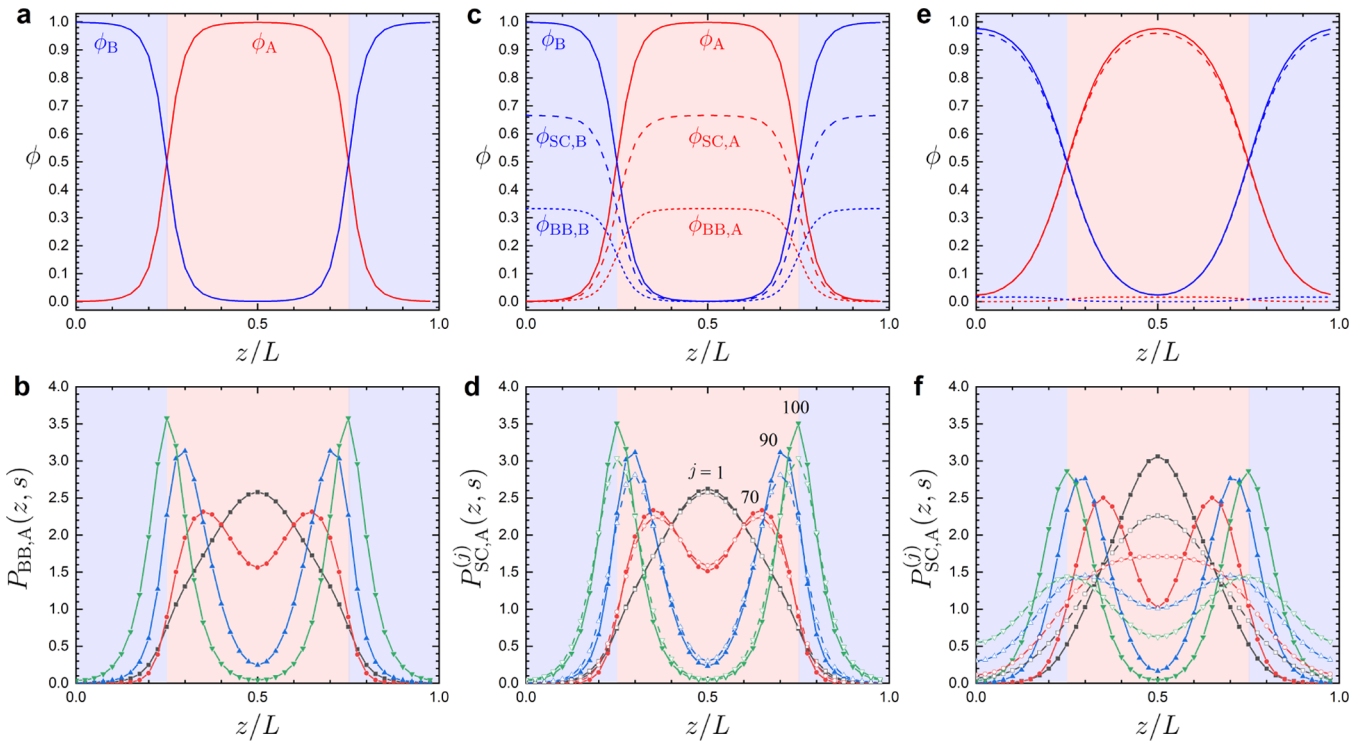

Figure 3. Density profiles and positional probability distributions for (a, b) linear diblock copolymers, (c, d) crewcut bottlebrushes, and (e, f) hairy bottlebrushes. The density profiles (top row) show all A-type segments (ϕ_A), all B-type segments (ϕ_B), A-type side chains ($\phi_{SC,A}$), B-type side chains ($\phi_{SC,B}$), A-type backbone ($\phi_{BB,A}$), and B-type backbone ($\phi_{BB,B}$). The positional probability distributions (bottom row) are the j = 1 (black), 70 (red), 90 (blue), and 100 (green) side chains, respectively, of the bottlebrushes at the free end s = 0 (dashed lines) and the grafting point at $s = N_{SC}$ (solid lines). The corresponding data for the linear diblocks are the location of the backbone segments at those grafting points. All data were obtained for f_A = 0.5. The linear diblock data correspond to χN = 36 and produced a lamellar period $L = 1.904bN_{BB}^{1/2}$. The bottlebrush data used n_{SC} = 200 and χN_{tot} = 36. The crewcut bottlebrushes used α = 0.01 and χ = 12, producing $L = 1.954bN_{BB}^{1/2}$, while the hairy bottlebrushes used α = 0.3 and χ = 0.59, producing $L = 2.619bN_{BB}^{1/2}$.

https://doi.org/10.1021/acs.macromol.1c01654
Macromolecules 2021, 54, 9063−9070

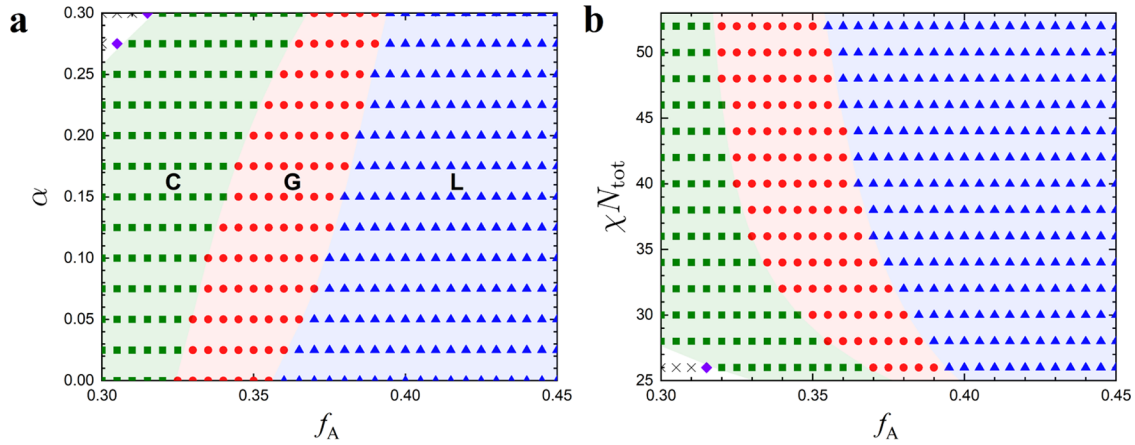

Figure 4. Phase diagrams at fixed (a) χN_{tot} = 26 and (b) α = 0.3. The symbols and labels are the same as in Figure 2.

L. The detailed calculations for the segmental distributions and the overall density profile ϕ's are explained in SI Section A.

Figure 3d reveals that the free ends of side chains are closely distributed around the corresponding grafting points on the backbone, with the overall density profiles of the A- and B-type segments being almost identical to those of linear diblock copolymers (Figure 3a,3c). The results imply that despite the high grafting density, the crewcut bottlebrush hardly stretches the backbone due to the neglected excluded volume effect in SCFT but they primarily increase the volume of the backbone. Taking the previous results together, the dominant effect of grafting crewcut side chains is increasing effective segregation strength by thickening the backbone and thus adding extra segregating segments at interfaces. They also indicate that, in the crewcut bottlebrush regime, the entropic contribution of side chains to the free energy has little impact on the phase stability of diblock copolymers even when the total volume fraction of grafts is comparable to the backbone. For example, there are twice as many graft segments as backbone segments when α = 0.01, as seen in the density profiles in Figure 3c but the general trend is not impacted by a large number of grafts. As the graft length keeps increasing, however, the difference of lamellar period between linear diblock copolymers and bottlebrush polymers grows, showing the crossover from the bottlebrush regime where the effective effect is increasing the backbone volumes, as seen in Figure S5.

To disentangle the effects of increasing graft length and overall segregation strength, we also constructed two phase diagrams at fixed values of χN_{tot} and α in Figure 4. Figure 4a shows a phase diagram analogous to Figure 2 but obtained at fixed χN_{tot} = 26 by adjusting χ, which enables investigation of the hairy bottlebrush regime as α increases. Note that N_{tot} varies with α as $N_{tot} = N_{BB}(1 + n_{SC}\alpha)$. In contrast to crewcut bottlebrush polymers, hairy bottlebrushes exhibit some distinct differences from the linear diblock copolymers. As the side-chain length keeps increasing, the ordered phase boundaries are slightly shifted to high-volume fractions of A, with the emergence of spherical and disordered phases over the parameter ranges studied here. This behavior indicates reduced segregation due to the decrease in χ, and the trend of narrowing stability regions for ordered phases is similar to that observed in the weakly segregated regime of the conventional diblock copolymer phase diagram. However, the degree of phase boundary shift is very small (Δf_A = 0.035) relative to the large architectural variation ($\Delta\alpha$ = 0.3). Additional results at a higher value of χN_{tot} = 36 (Figure S3) further confirm that the hairy bottlebrush architecture hardly impacts the stability of the ordered phases.

While there is little change in the locations of phase boundaries, the self-assembled morphologies of hairy bottlebrush polymers differ significantly from those of diblock copolymers due to changes in the packing of long side chains. As seen by comparing the density profiles of Figure 3a,3e, the lamellar morphology self-assembled by hairy bottlebrush polymers exhibits a much wider AB interface and the domain spacing is significantly increased (by 37.6%). In addition, as indicated from the segmental probability densities (Figure 3, bottom row), the backbone configurations of hairy bottlebrush polymers are apparently different from those of crewcut bottlebrush polymers, while the crewcut bottlebrush architectures are very similar to the linear diblocks. In SCFT, the incompressibility is treated within the mean-field approximation, so it is incapable of accounting for the steric interaction effect of the densely grafted long side chains. The steric interactions ignored by SCFT may become important for the larger values of α. Considering a large amount of hairy graft segments, backbone conformations in realistic bottlebrush block polymers would be more significantly stretched than the SCFT prediction as a result of steric congestions of grafts.

In hairy bottlebrush polymer melts, most of the segment densities come from the grafts, so their entropic contribution to the free energy plays a significant role in the self-assembly. Therefore, the longer side chains with lower χ can more easily make a broad interface by distributing free ends deeper into opposite domains, as shown in segment distributions of crewcut and hairy bottlebrush polymers (Figure 3d,3f). The distribution of side chains into opposite domains makes the backbone segments far from the interface stretch, which can explain the increased domain spacing. The broad A/B interface can be fully anticipated when considering the hairy bottlebrush polymer melts as approximations for A−B polymer blends in which the interfacial width varies as $\chi^{-0.5}$ according to the analytical expression proposed by Helfand and Tagami.[47] For realistic bottlebrush block polymers with a limited degree of polymerization, however, we expect that strong steric interactions will induce radial stretching of side chains away from the backbone, which affects monomer packing and microphase segregation, and thus the interfacial width would be less broad than our SCFT prediction indicates.

https://doi.org/10.1021/acs.macromol.1c01654
Macromolecules 2021, 54, 9063−9070

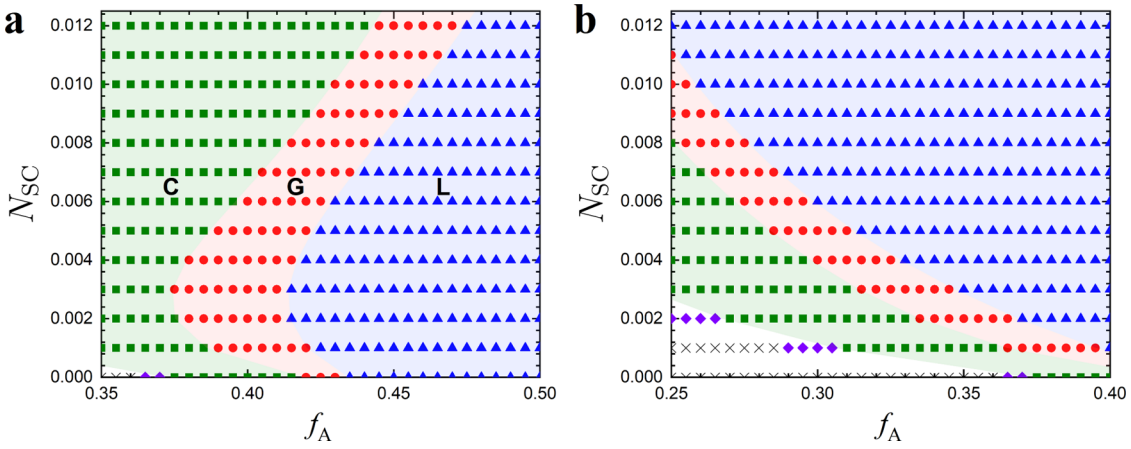

Figure 5. Phase diagrams of (a) coil(A)−bottlebrush(B) polymer and (b) bottlebrush(A)−coil(B) polymer, both at $\chi = 12$. At a fixed composition fraction f_A, the backbone length is proportional to the side-chain length N_{SC} since the new backbone length $N_{BB}^{coil-brush}$, written in terms of the original bottlebrush backbone length N_{BB}, is $N_{BB}^{coil-brush} = N_{BB} + n_{SC}f_A N_{SC}$ for coil(A)−bottlebrush(B) polymers and $N_{BB}^{brush-coil} = N_{BB} + n_{SC}(1 - f_A)$ N_{SC} for bottlebrush(A)−coil(B) polymers. The same symbols and labels are used as in Figures 2 and 4.

Figure 4b shows how the A/B interaction strength, χ, affects the stability of ordered phases in the hairy bottlebrush polymer ($\alpha = 0.3$) melts. Increasing χ leads to shifts of the phase boundary to lower f_A values compared to those at $\chi N_{tot} = 26$, which is similar to the phase behavior commonly observed in diblock copolymers for increasing χN. In the self-assembly of diblock copolymers, a well-known physical principle is that competition between the stretching penalties of the A and B blocks determines the geometry of microstructures. For the case of compositionally asymmetric diblock copolymers, the total stretching energy can be minimized by curving the interface toward the minority domain to relax the majority blocks at the expense of stretching the minority blocks. As block composition becomes more asymmetric, higher interfacial curvature is preferred, and this tendency is confirmed by the sequence of equilibrium structures at intermediate segregation, lamella → gyroid → cylinder → sphere, as f_A goes from 0.5 to either 0 or 1. In high segregation, both A and B bottlebrush blocks are more stretched than in low segregation, so the competition of stretching penalties between A and B bottlebrush blocks will become a dominant factor determining the phase boundary locations, which can be analyzed by the strong-stretching theory.[48,49] We can also speculate that the phase boundaries in Figure 4a are not significantly impacted despite the different distribution of the monomers because the side-chain length has little influence on the effective competition between stretching penalties of blocks in the majority and minority domains and thus on the tendency to accommodate interfacial curvature.

To summarize the results thus far, the double gyroid phase window of crewcut bottlebrush polymers can be predicted with the results for linear diblock copolymers at equivalent χN, where $N = N_{tot}$ is the total degree of polymerization, and the gyroid window is remarkably robust to architectural variation from the linear diblock to the hairy bottlebrush diblock copolymer. Our finding is consistent with the recent analytic theory, which predicts that in strong segregation limit, S/C and C/L phase boundaries of architecturally and elastically symmetric bottlebrush block polymers have the same positions in volume fraction as those of diblock copolymers.[49] Since the latter argument is based on the strong-stretching theory and excludes complex network phases, our work extends their conclusion to both weak segregation and complex network phases.

Architecturally Asymmetric Bottlebrush Polymers. We now examine the effect of architectural asymmetry on phase behaviors with the coil−bottlebrush architectures illustrated in Figure 1. They are made by taking all A- or B-type side chains in crewcut bottlebrush polymers of backbone length N_{BB} used in Figure 2 and putting them at the relevant end of the backbone. In this model, for a given number of side chains determined by f_A, i.e., $n_{SC}(1 - f_A)$ for coil(A)−bottlebrush(B) polymers and $n_{SC}f_A$ for bottlebrush(A)−coil(B) polymers, the side-chain length N_{SC} proportionally increases the length difference between A and B backbone blocks in the coil−bottlebrush polymer. As a result, N_{SC} can be used to tune architectural asymmetry, which then affects the self-assembly behavior. Note that when $N_{SC} \to 0$, the molecular architecture reduces to linear−linear diblocks, which have no space-filling asymmetry. The phase diagram of coil(A)−bottlebrush(B) polymers in Figure 5a indicates that, when the minority domains are coils, the gyroid phase window is considerably deflected toward high-volume fractions of A. In contrast, when the minority domains are bottlebrushes, the gyroid window width is a little narrower compared to the counterpart coil−bottlebrush polymers and shifts to low-volume fractions of A, as shown in Figure 5b.

Similar trends in the deflection of the gyroid phase window were found in previous studies of conformationally asymmetric block copolymers, for example, diblock copolymers where the statistical segment length differs[50] and the asymmetric miktoarm star polymer A_mB_n, where the number of arms differs between the two blocks ($m \neq n$).[51,52] In these studies, the most obvious effect of conformational asymmetry was to shift the phase boundaries. The equivalent effect in two polymer systems was theoretically proven earlier by Milner, who derived the conformational asymmetry parameter, combining the overall effect of both architectural and elastic asymmetries with the strong-stretching theory.[53] However, his derivation was based on the assumptions of strong segregation and multiarm architectures including diblocks, which complicates the derivations for probing other complex network phases.[54,55] The equivalence of the conformational asymmetry effects was recently examined by Li and Liu in their SCFT

https://doi.org/10.1021/acs.macromol.1c01654
Macromolecules 2021, 54, 9063−9070

study for the phase diagram over both intermediate and strong segregation ranges.[52]

Our results can be rationalized as emerging from the extreme conformational asymmetry between the coil blocks and the bottlebrush blocks. The crewcut bottlebrush block is a relatively short and thick coil, which is more difficult to stretch than a linear coil block for the same extension. Thus, the competition between the stretching penalties affects the tendency to curve the AB interface, which results in shifts of the phase boundaries. Specifically, if the coil blocks are the minority, there is a tendency to form spontaneous curvature toward the coil blocks, thereby relaxing the bottlebrush blocks through the large space near interfaces, at the cost of stretching the coil blocks, leading to deflection of phase boundaries. On the other hand, when the brush blocks are the minority, there are entropic penalties associated with stretching the bottlebrush blocks inside the minority domains, so a curved geometry is unfavorable. For the double gyroid phase, packing frustration is highest at the center of the gyroid nodes,[40] so a long coil is more favorable to fill the space than bottlebrush block, which partially explains the somewhat wider gyroid window for the phase diagram of coil(A)−bottlebrush(B) polymers than that of bottlebrush(A)−coil(B) polymers.

In this work, we did not consider other spherical phases, such as the Frank−Kasper σ phase and A15 phase, but these phases have been reported in experiments with coil−bottlebrush polymers[56,57] and these should prove to be fruitful avenues for future research. Our study of the double gyroid phase adds to the understanding of the architectural asymmetry effect inherent in coil−bottlebrush polymers, extending the earlier theoretical predictions[49,54,55] to both bottlebrush architecture and complex network phase formation in the intermediate segregation regime.

We have considered here only the simplest variant on the bottlebrush diblock polymer, i.e., coil−bottlebrush polymers, but there are numerous possible molecular designs that might further amplify the effects seen here. For example, as suggested in the recent research on $A(AB)_n$ miktoarm star copolymers,[58] packing frustration near the saddle surface of the double gyroid structure could be relieved by the cost of AB mixing near the interface. Double gyroid has relatively low interfacial curvature, so it would be interesting to explore the phase stability with other types of coil−bottlebrush block architectures, for example, by creating a partial bottlebrush block in the coil part next to the chemically different bottlebrush block. Such an extraordinary coil−bottlebrush block architecture could improve AB mixing near the saddle surface and also relieve packing frustration at the center of nodes by long coil blocks, possibly resulting in stabilization of the gyroid region.

CONCLUDING REMARKS

In summary, we have shown here that double gyroid phases are not only present in bottlebrush polymers but their stability window can be increased by tailoring the architecture. The similarity of phase behaviors between linear diblock polymers and crewcut bottlebrush polymers suggests that other complex phases observed in linear diblock copolymers, such as Fddd, perforated lamellae, and double diamond, could be observed as well in sufficiently long bottlebrush diblock copolymers. The results were obtained using a mean-field approximation and the Gaussian chain model, which are a logical starting point used in other related works,[24−26,38,39] but may pose some challenges in translation to experiments.

A particular limitation of the model is that the density fluctuations restricted by harsh excluded volume repulsion are treated solely through incompressibility within the mean-field approximation and it does not capture the crowding of the side chains. The SCFT community has dealt with this limitation by adopting wormlike chain models and fitting the persistence length to experimental measurement.[24,25,43] However, adjusting the molecular parameter in this modeling requires experimentally available data, such as domain spacing, and thus is not predictive. Another possible approach is field-theoretic simulation (FTS),[59−61] which is beyond the mean-field theory. Using complex Langevin sampling technique for fully fluctuating fields, Panagiotou et al. demonstrated the effect of grafting density in bottlebrush homopolymers on phase transition from an isotropic to a nematic state, which supports that FTS is capable of handling steric interactions.[62] However, FTS has its own challenges in high computational cost and numerical instability causing the fields to diverge.

It would be helpful to inform the community of SCFT's incapability to account for the excluded volume interaction effect through local incompressibility conditions by showing the calculation with a highly grafted bottlebrush regime. Our results for the crewcut bottlebrush SCFT with a grafting density of up to 200 side chains per backbone suggest that the physics of steric interaction in bottlebrush polymers indeed is not captured in the mean-field limit. To advance realistic calculation on finite molecular weight bottlebrush polymers and pursue the theoretical calculation associated with complex network phases, additional improvement in SCFT bottlebrush models is needed.

Nevertheless, our SCFT predictions of network phases can be compared with experiments using long bottlebrush block polymers relative to the side chains. For the long densely grafted bottlebrush polymer, the steric-induced persistence length would be small relative to backbone length, and this is the most promising regime for an agreement between theory and experiment. In that regard, the degree of the backbone rigidity and its impact on the stability of network phases in long bottlebrush polymers should be examined by experiments and theories, and SCFT is an appropriate first step to providing concrete predictions along with experiments. Our work demonstrates the potential for tailoring molecular design in bottlebrush block polymers to manipulate phase behaviors, creating a new opportunity for making advanced materials with desired network nanostructures.

ASSOCIATED CONTENT

Supporting Information

The Supporting Information is available free of charge at https://pubs.acs.org/doi/10.1021/acs.macromol.1c01654.

SCFT formalism and simulation details, additional phase diagram results, and free energy and lamellar period data (PDF)

AUTHOR INFORMATION

Corresponding Author

Kevin D. Dorfman − *Department of Chemical Engineering and Materials Science, University of Minnesota—Twin Cities, Minneapolis, Minnesota 55455, United States;* orcid.org/0000-0003-0065-5157; Email: dorfman@umn.edu

https://doi.org/10.1021/acs.macromol.1c01654
Macromolecules 2021, 54, 9063−9070

Authors

So Jung Park − *Department of Chemical Engineering and Materials Science, University of Minnesota—Twin Cities, Minneapolis, Minnesota 55455, United States;* orcid.org/0000-0002-3003-6501

Guo Kang Cheong − *Department of Chemical Engineering and Materials Science, University of Minnesota—Twin Cities, Minneapolis, Minnesota 55455, United States*

Frank S. Bates − *Department of Chemical Engineering and Materials Science, University of Minnesota—Twin Cities, Minneapolis, Minnesota 55455, United States;* orcid.org/0000-0003-3977-1278

Complete contact information is available at: https://pubs.acs.org/10.1021/acs.macromol.1c01654

Notes

The authors declare no competing financial interest.

■ ACKNOWLEDGMENTS

The authors thank Prof. David C. Morse for assistance with the SCFT code. This work was supported primarily by the National Science Foundation through the University of Minnesota MRSEC under Award Number DMR-2011401. The Minnesota Supercomputing Institute (MSI) at the University of Minnesota provided resources that contributed to the research results reported within this paper.

■ REFERENCES

(1) Feng, H.; Lu, X.; Wang, W.; Kang, N.-G.; Mays, J. W. Block Copolymers: Synthesis, Self-Assembly, and Applications. *Polymers* **2017**, *9*, 494.

(2) Bates, C. M.; Bates, F. S. 50th Anniversary Perspective: Block Polymers−Pure Potential. *Macromolecules* **2017**, *50*, 3−22.

(3) Xia, Y.; Kornfield, J. A.; Grubbs, R. H. Efficient Synthesis of Narrowly Dispersed Brush Polymers via Living Ring-Opening Metathesis Polymerization of Macromonomers. *Macromolecules* **2009**, *42*, 3761−3766.

(4) Lin, T.-P.; Chang, A. B.; Chen, H.-Y.; Liberman-Martin, A. L.; Bates, C. M.; Voegtle, M. J.; Bauer, C. A.; Grubbs, R. H. Control of Grafting Density and Distribution in Graft Polymers by Living Ring-Opening Metathesis Copolymerization. *J. Am. Chem. Soc.* **2017**, *139*, 3896−3903.

(5) Verduzco, R.; Li, X.; Pesek, S. L.; Stein, G. E. Structure, function, self-assembly, and applications of bottlebrush copolymers. *Chem. Soc. Rev.* **2015**, *44*, 2405−2420.

(6) Xie, G.; Martinez, M. R.; Olszewski, M.; Sheiko, S. S.; Matyjaszewski, K. Molecular Bottlebrushes as Novel Materials. *Biomacromolecules* **2019**, *20*, 27−54.

(7) Rzayev, J. Molecular bottlebrushes: New opportunities in nanomaterials fabrication. *ACS Macro Lett.* **2012**, *1*, 1146−1149.

(8) Liang, H.; Cao, Z.; Wang, Z.; Sheiko, S. S.; Dobrynin, A. V. Combs and Bottlebrushes in a Melt. *Macromolecules* **2017**, *50*, 3430−3437.

(9) Paturej, J.; Sheiko, S. S.; Panyukov, S.; Rubinstein, M. Molecular structure of bottlebrush polymers in melts. *Sci. Adv.* **2016**, *2*, No. e1601478.

(10) Hu, M.; Xia, Y.; McKenna, G. B.; Kornfield, J. A.; Grubbs, R. H. Linear rheological response of a series of densely branched brush polymers. *Macromolecules* **2011**, *44*, 6935−6943.

(11) Sveinbjörnsson, B. R.; Weitekamp, R. A.; Miyake, G. M.; Xia, Y.; Atwater, H. A.; Grubbs, R. H. Rapid self-assembly of brush block copolymers to photonic crystals. *Proc. Natl. Acad. Sci. U.S.A.* **2012**, *109*, 14332−14336.

(12) Rzayev, J. Synthesis of polystyrene-polylactide bottlebrush block copolymers and their melt self-assembly into large domain nanostructures. *Macromolecules* **2009**, *42*, 2135−2141.

(13) Bolton, J.; Bailey, T. S.; Rzayev, J. Large Pore Size Nanoporous Materials from the Self-Assembly of Asymmetric Bottlebrush Block Copolymers. *Nano Lett.* **2011**, *11*, 998−1001.

(14) Fei, H.-F.; Yavitt, B. M.; Hu, X.; Kopanati, G.; Ribbe, A.; Watkins, J. J. Influence of Molecular Architecture and Chain Flexibility on the Phase Map of Polystyrene-block-poly(dimethylsiloxane) Brush Block Copolymers. *Macromolecules* **2019**, *52*, 6449−6457.

(15) Gai, Y.; Song, D.-P.; Yavitt, B. M.; Watkins, J. J. Polystyrene-block-poly(ethylene oxide) Bottlebrush Block Copolymer Morphology Transitions: Influence of Side Chain Length and Volume Fraction. *Macromolecules* **2017**, *50*, 1503−1511.

(16) Miyake, G. M.; Weitekamp, R. A.; Piunova, V. A.; Grubbs, R. H. Synthesis of isocyanate-based brush block copolymers and their rapid self-assembly to infrared-reflecting photonic crystals. *J. Am. Chem. Soc.* **2012**, *134*, 14249−14254.

(17) Liberman-Martin, A. L.; Chu, C. K.; Grubbs, R. H. Application of Bottlebrush Block Copolymers as Photonic Crystals. *Macromol. Rapid Commun.* **2017**, *38*, No. 1700058.

(18) Macfarlane, R. J.; Kim, B.; Lee, B.; Weitekamp, R. A.; Bates, C. M.; Lee, S. F.; Chang, A. B.; Delaney, K. T.; Fredrickson, G. H.; Atwater, H. A.; Grubbs, R. H. Improving brush polymer infrared one-dimensional photonic crystals via linear polymer additives. *J. Am. Chem. Soc.* **2014**, *136*, 17374−17377.

(19) Miyake, G. M.; Piunova, V. A.; Weitekamp, R. A.; Grubbs, R. H. Precisely tunable photonic crystals from rapidly self-assembling brush block copolymer blends. *Angew. Chem., Int. Ed.* **2012**, *51*, 11246−11248.

(20) Cheng, L.-C.; Gadelrab, K. R.; Kawamoto, K.; Yager, K. G.; Johnson, J. A.; Alexander-Katz, A.; Ross, C. A. Templated Self-Assembly of a PS-*Branch*-PDMS Bottlebrush Copolymer. *Nano Lett.* **2018**, *18*, 4360−4369.

(21) Lu, X.; Tran, T.-H.; Jia, F.; Tan, X.; Davis, S.; Krishnan, S.; Amiji, M. M.; Zhang, K. Providing Oligonucleotides with Steric Selectivity by Brush-Polymer-Assisted Compaction. *J. Am. Chem. Soc.* **2015**, *137*, 12466−12469.

(22) Johnson, J. A.; Lu, Y. Y.; Burts, A. O.; Xia, Y.; Durrell, A. C.; Tirrell, D. A.; Grubbs, R. H. Drug-loaded, bivalent-bottle-brush polymers by graft-through ROMP. *Macromolecules* **2010**, *43*, 10326−10335.

(23) Gu, W.; Huh, J.; Hong, S. W.; Sveinbjornsson, B. R.; Park, C.; Grubbs, R. H.; Russell, T. P. Self-Assembly of Symmetric Brush Diblock Copolymers. *ACS Nano* **2013**, *7*, 2551−2558.

(24) Dalsin, S. J.; Rions-Maehren, T. G.; Beam, M. D.; Bates, F. S.; Hillmyer, M. A.; Matsen, M. W. Bottlebrush Block Polymers: Quantitative Theory and Experiments. *ACS Nano* **2015**, *9*, 12233−12245.

(25) Chen, Y.; Zhang, X.; Jiang, Y. The influence of side-chain conformations on the phase behavior of bottlebrush block polymers. *Soft Matter* **2020**, *16*, 8047−8056.

(26) Levi, A. E.; Lequieu, J.; Horne, J. D.; Bates, M. W.; Ren, J. M.; Delaney, K. T.; Fredrickson, G. H.; Bates, C. M. Miktoarm Stars via Grafting-Through Copolymerization: Self-Assembly and the Star-to-Bottlebrush Transition. *Macromolecules* **2019**, *52*, 1794−1802.

(27) Lin, T.-P.; Chang, A. B.; Luo, S.-X.; Chen, H.-Y.; Lee, B.; Grubbs, R. H. Effects of Grafting Density on Block Polymer Self-Assembly: From Linear to Bottlebrush. *ACS Nano* **2017**, *11*, 11632−11641.

(28) Runge, M. B.; Bowden, N. B. Synthesis of high molecular weight comb block copolymers and their assembly into ordered morphologies in the solid state. *J. Am. Chem. Soc.* **2007**, *129*, 10551−10560.

(29) Xia, Y.; Olsen, B. D.; Kornfield, J. A.; Grubbs, R. H. Efficient synthesis of narrowly dispersed brush copolymers and study of their assemblies: The importance of side chain arrangement. *J. Am. Chem. Soc.* **2009**, *131*, 18525−18532.

(30) Hong, S. W.; Gu, W.; Huh, J.; Sveinbjornsson, B. R.; Jeong, G.; Grubbs, R. H.; Russell, T. P. On the Self-Assembly of Brush Block Copolymers in Thin Films. *ACS Nano* **2013**, *7*, 9684−9692.

(31) Jiang, L.; Nykypanchuk, D.; Pastore, V. J.; Rzayev, J. Morphological Behavior of Compositionally Gradient Polystyrene−Polylactide Bottlebrush Copolymers. *Macromolecules* **2019**, *52*, 8217−8226.
(32) Gin, D. L.; Bara, J. E.; Noble, R. D.; Elliott, B. J. Polymerized lyotropic liquid crystal assemblies for membrane applications. *Macromol. Rapid Commun.* **2008**, *29*, 367−389.
(33) Li, L.; Schulte, L.; Clausen, L. D.; Hansen, K. M.; Jonsson, G. E.; Ndoni, S. Gyroid nanoporous membranes with tunable permeability. *ACS Nano* **2011**, *5*, 7754−7766.
(34) Jackson, G. L.; Perroni, D. V.; Mahanthappa, M. K. Roles of Chemical Functionality and Pore Curvature in the Design of Nanoporous Proton Conductors. *J. Phys. Chem. B* **2017**, *121*, 9429−9436.
(35) Ichikawa, T.; Kato, T.; Ohno, H. 3D continuous water nanosheet as a gyroid minimal surface formed by bicontinuous cubic liquid-crystalline zwitterions. *J. Am. Chem. Soc.* **2012**, *134*, 11354−11357.
(36) Saranathan, V.; Osuji, C. O.; Mochrie, S. G.; Noh, H.; Narayanan, S.; Sandy, A.; Dufresne, E. R.; Prum, R. O. Structure, function, and self-assembly of single network gyroid ($I4_132$) photonic crystals in butterfly wing scales. *Proc. Natl. Acad. Sci. U.S.A.* **2010**, *107*, 11676−11681.
(37) Urbas, A. M.; Maldovan, M.; DeRege, P.; Thomas, E. L. Bicontinuous cubic block copolymer photonic crystals. *Adv. Mater.* **2002**, *14*, 1850−1853.
(38) Kawamoto, K.; Zhong, M.; Gadelrab, K. R.; Cheng, L.-C.; Ross, C. A.; Alexander-Katz, A.; Johnson, J. A. Graft-through Synthesis and Assembly of Janus Bottlebrush Polymers from A-Branch-B Diblock Macromonomers. *J. Am. Chem. Soc.* **2016**, *138*, 11501−11504.
(39) Lequieu, J.; Quah, T.; Delaney, K. T.; Fredrickson, G. H. Complete Photonic Band Gaps with Nonfrustrated ABC Bottlebrush Block Polymers. *ACS Macro Lett.* **2020**, *9*, 1074−1080.
(40) Matsen, M. W.; Bates, F. S. Origins of Complex Self-Assembly in Block Copolymers. *Macromolecules* **1996**, *29*, 7641−7644.
(41) Matsen, M. W. The standard Gaussian model for block copolymer melts. *J. Phys.: Condens. Matter* **2002**, *14*, R21−R47.
(42) Khandpur, A. K.; Förster, S.; Bates, F. S.; Hamley, I. W.; Ryan, A. J.; Bras, W.; Almdal, K.; Mortensen, K. Polyisoprene-Polystyrene Diblock Copolymer Phase Diagram near the Order-Disorder Transition. *Macromolecules* **1995**, *28*, 8796−8806.
(43) Chang, A. B.; Bates, C. M.; Lee, B.; Garland, C. M.; Jones, S. C.; Spencer, R. K. W.; Matsen, M. W.; Grubbs, R. H. Manipulating the ABCs of self-assembly via low-χ block polymer design. *Proc. Natl. Acad. Sci. U.S.A.* **2017**, *114*, 6462−6467.
(44) Jiang, Y.; Chen, J. Z. Y. Influence of chain rigidity on the phase behavior of wormlike diblock copolymers. *Phys. Rev. Lett.* **2013**, *110*, No. 138305.
(45) Arora, A.; Qin, J.; Morse, D. C.; Delaney, K. T.; Fredrickson, G. H.; Bates, F. S.; Dorfman, K. D. Broadly Accessible Self-Consistent Field Theory for Block Polymer Materials Discovery. *Macromolecules* **2016**, *49*, 4675−4690.
(46) Cheong, G. K.; Chawla, A.; Morse, D. C.; Dorfman, K. D. Open-source code for self-consistent field theory calculations of block polymer phase behavior on graphics processing units. *Eur. Phys. J. E* **2020**, *43*, No. 15.
(47) Helfand, E.; Tagami, Y. Theory of the interface between immiscible polymers. II. *J. Chem. Phys.* **1972**, *56*, No. 3592.
(48) Semenov, A. N. Contribution to the Theory of Microphase Layering in Block-Copolymer Melts. *J. Exp. Theor. Phys.* **1985**, *61*, 733−742.
(49) Zhulina, E. B.; Sheiko, S. S.; Dobrynin, A. V.; Borisov, O. V. Microphase Segregation in the Melts of Bottlebrush Block Copolymers. *Macromolecules* **2020**, *53*, 2582−2593.
(50) Matsen, M. W.; Bates, F. S. Conformationally Asymmetric Block Copolymers. *J. Polym. Sci., Part B: Polym. Phys.* **1997**, *35*, 945−952.
(51) Xie, N.; Li, W.; Qiu, F.; Shi, A.-C. σ Phase Formed in Conformationally Asymmetric AB-Type Block Copolymers. *ACS Macro Lett.* **2014**, *3*, 906−910.
(52) Li, W.; Liu, Y.-X. Simplicity in mean-field phase behavior of two-component miktoarm star copolymers. *J. Chem. Phys.* **2021**, *154*, No. 014903.
(53) Milner, S. T. Chain Architecture and Asymmetry in Copolymer Microphases. *Macromolecules* **1994**, *27*, 2333−2335.
(54) Olmsted, P. D.; Milner, S. T. Strong Segregation Theory of Bicontinuous Phases in Block Copolymers. *Macromolecules* **1998**, *31*, 4011−4022.
(55) Olmsted, P. D.; Milner, S. T. Strong-Segregation Theory of Bicontinuous Phases in Block Copolymers. *Phys. Rev. Lett.* **1994**, *72*, 936−939.
(56) Chang, A. B.; Bates, F. S. Impact of Architectural Asymmetry on Frank Kasper Phase Formation in Block Polymer Melts. *ACS Nano* **2020**, *14*, 11463−11472.
(57) Bates, M. W.; Lequieu, J.; Barbon, S. M.; Lewis, R. M.; Delaney, K. T.; Anastasaki, A.; Hawker, C. J.; Fredrickson, G. H.; Bates, C. M. Stability of the A15 phase in diblock copolymer melts. *Proc. Natl. Acad. Sci. U.S.A.* **2019**, *116*, 13194−13199.
(58) Li, C.; Dong, Q.; Li, W. Largely Tunable Asymmetry of Phase Diagrams of $A(AB)_n$ Miktoarm Star Copolymer. *Macromolecules* **2020**, *53*, 10907−10917.
(59) Delaney, K. T.; Fredrickson, G. H. Recent Developments in Fully Fluctuating Field-Theoretic Simulations of Polymer Melts and Solutions. *J. Phys. Chem. B* **2016**, *120*, 7615−7634.
(60) Audus, D. J.; Delaney, K. T.; Ceniceros, H. D.; Fredrickson, G. H. Comparison of pseudospectral algorithms for field-theoretic simulations of polymers. *Macromolecules* **2013**, *46*, 8383−8391.
(61) Koski, J.; Chao, H.; Riggleman, R. A. Field theoretic simulations of polymer nanocomposites. *J. Chem. Phys.* **2013**, *139*, No. 244911.
(62) Panagiotou, E.; Delaney, K. T.; Fredrickson, G. H. Theoretical prediction of an isotropic to nematic phase transition in bottlebrush homopolymer melts. *J. Chem. Phys.* **2019**, *151*, No. 094901.

https://doi.org/10.1021/acs.macromol.1c01654
Macromolecules 2021, 54, 9063−9070